Tectonophysics 554-557 (2012) 169–184

Contents lists available at SciVerse ScienceDirect

Tectonophysics

journal homepage: www.elsevier.com/locate/tecto

Interseismic crustal deformation of frontal thrust fault system in the Chiayi–Tainan area, Taiwan

Min-Chien Tsai [a,c], Shui-Beih Yu [b,*], Ya-Ju Hsu [b], Horng-Yue Chen [b], How-Wei Chen [a]

[a] Institute of Geophysics, National Central University, Chungli, Taoyuan, Taiwan
[b] Institute of Earth Sciences, Academia Sinica, Nankang, Taipei, Taiwan
[c] Seismological Center, Central Weather Bureau, Taipei, Taiwan

ARTICLE INFO

Article history:
Received 1 September 2011
Received in revised form 3 May 2012
Accepted 15 May 2012
Available online 26 May 2012

Keywords:
GPS survey
Frontal thrust faults
Dislocation model
Interseismic crustal deformation

ABSTRACT

We derive a velocity field using GPS data between 1993 and 2007 in the Chiayi–Tainan area located in the deformation front of the Taiwan mountain belt. The crustal motion with respect to Penghu shows large velocities of about 33–44 mm/yr in the west-northwest to west directions in the Western Foothills and the velocities decrease westward to 0–5 mm/yr in the coastal area. Significant uplift rates of 5–20 mm/yr are observed at sites to the east of the Jiuchiunken–Muchiliao–Liuchia Fault (JMLF) system. We use a block model, a buried dislocation model, and a two-dimensional fault model to invert for fault geometries and slip rates on major frontal thrust faults. Modeling results from a block model show the inferred long-term slip rate of 42 mm/yr in the direction of 280° and the maximum back-slip rate of 38 mm/yr on a 23° east dipping fault extending to 13 km at depth. On the other hand, the buried dislocation model results in a horizontal décollement at a depth of 8 km with a uniform slip rate of 41.6 mm/yr. If we connect the top edge of décollement to the surface trace of JMLF as a potential future rupture, a 22° east-dipping fault is required. Results from both block model and buried dislocation model suggest the JMLF is nearly fully locked. The results of two-dimensional fault models show the frontal thrust faults have slip rates of less than 2 mm/yr at shallow depths and the inferred décollement is sub-horizontal (5°–7°) at a depth of 10 km with slip rates of 44–46 mm/yr. Results of various approaches show general agreement on fault geometries and slip rates and reveal that the frontal thrust fault system has a high potential for large earthquakes.
© 2012 Elsevier B.V. All rights reserved.

1. Introduction

The modern technique of global positioning system (GPS) provides an efficient tool to study active tectonics and geodynamics. Combining data from continuous GPS array and survey-mode GPS sites, we are able to estimate fault-slip rates, infer fault geometry, and assess regional seismic hazard (Bock, 1994; Dixon, 1991; Hager et al., 1991; Hudnut, 1995). The first GPS survey in Taiwan was conducted in 1990 and aimed at studying regional tectonics and fault activities. Taiwan is situated at an active continental margin wherein numerous thrust faults and folds had formed due to the collision between the Luzon arc and the Chinese continental margin. The convergence rate across the Taiwan mountain belt is about 80 mm/yr based on GPS measurements (Hickman et al., 2002; Hsu et al., 2009; Yu et al., 1997; 1999). Approximately half of the plate convergence rate is accommodated on the fold and thrust belt of southwestern Taiwan. The major frontal thrusts in this area from west to east are: the Chiayi Fault, Jiuchiunken–Muchiliao–Liuchia Fault system (JMLF), and Tachienshan–Chukou Fault (Fig. 1). These faults are likely to sole into a décollement at depths.

The high shortening rate of up to 40 mm/yr in the Chiayi–Tainan area makes it a key region to study how fault slip varies in space (Yu et al., 1997). This area is located to the southeast of the Peikang High, the Pre-Miocene basement on the Chinese continental margin (Fig. 1), and has experienced an east–west contraction due to the collision. In this region, a continuous GPS array composed of 46 stations is now in operation. Furthermore, 73 survey-mode sites mostly have been occupied at least once annually since 1993. We analyze GPS time series and estimate the velocity field between 1993 and 2007. Using these GPS data, seismic reflection profiles, and geological data, we aim to better estimate subsurface fault geometries and slip rates on frontal thrust fault systems in the Chiayi–Tainan area. The modeling results may shed a new light to understand complex fault structures and potential seismic hazard in the area.

2. Tectonic setting

The Taiwan mountain belt is formed by the oblique collision between the Philippine Sea Plate and the Eurasia Plate (Angelier, 1986). It exhibits different stages of the collision process from south

* Corresponding author at: Institute of Earth Sciences, Academia Sinica, P.O. Box 1-55, Nankang, Taipei 115, Taiwan. Tel.: +886 2 2783 9910x416; fax: +886 2 2783 9871.
E-mail address: yusb@earth.sinica.edu.tw (S.-B. Yu).

0040-1951/$ – see front matter © 2012 Elsevier B.V. All rights reserved.
doi:10.1016/j.tecto.2012.05.014

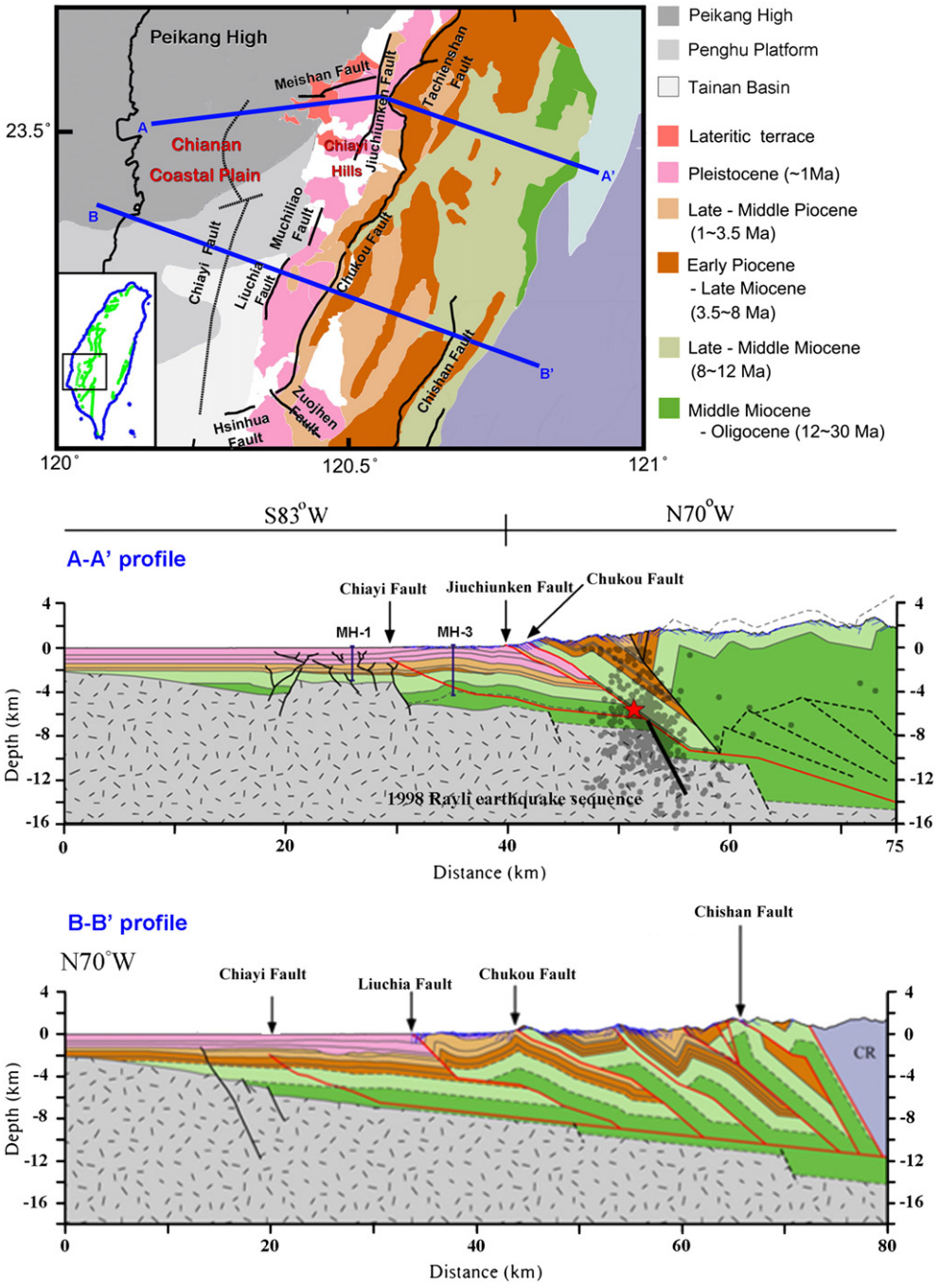

Fig. 1. Geological map and balanced geologic cross sections in the Chiayi–Tainan area. The color of each lithologic unit is shown on the right side of top panel. Different gray patterns denote locations of Miocene basement: Peikang High, Penghu Platform and Tainan Basin. The blue lines indicates the locations of two balanced geologic cross sections AA′ and BB′ shown at the bottom two panels.
Modified from Yang, 2007.

to north: pre-collisional with rapid and distributed convergence, collision and suturing, and post-collisional with collapse and extension (Lallemend and Tsein, 1997; Shyn et al., 2005). The ongoing collision is resisted by the Peikang High (Fig. 1), a Pre-Miocene basement, which acts as a buttress for advancing thrusts and creates a frontal thrust fault system parallel to the margin of the basement (Mouthereau and Petit, 2003; Tsan and Keng, 1968). At the eastern edge of the Peikang High, geometrical irregularity of the basement high is the most important factor that controls the geological development for each compartment Lin et al. (2003). The Peikang High plunges both southward and northward to form the east–west striking Meishan Fault in the Chiayi–Tainan area. The thin-skin thrusting was retarded by the ridge and resulted in the emergence of low angle thrust faults (Huang, 2003; Lacombe et al., 2001; Yang et al., 2006).

The Chiayi–Tainan area contains two different geological provinces, the Coastal Plain and Western Foothills, which is mainly comprised by Middle Miocene to Late Pleistocene formations (Ho, 2006). The strikes of rock formations are predominately north to northeast and a great portion is deformed along the folds and thrusts with dips to east or southeast. The intensity of deformation is decreasing from east to west (Ho, 1976; Suppe, 1980).

The major active faults in this area are: Meishan Fault, Jiuchiunken Fault, Muchiliao Fault, Liuchia Fault, Tachienshan Fault, and Chukou Fault (Fig. 1). We briefly summarize the features of these active faults

based on seismic reflections, geomorphology and GPS data. The dextral-slip Meishan Fault ruptured during the 1906 Meishan earthquake (M_L 7.1, Omori, 1907a,b; Lin et al., 2007). Seismic reflection data suggests that the Meishan Fault is a high-angle fault forming a flower structure, and terminates by the Jiuchiunken Fault to the east. The Jiuchiunken Fault is located on the eastern flank of Chiayi Hill (Fig. 1) and has been activated in Late Pleistocene. According to geological investigations, the fault strikes N20°E–N25°E with a dip of about 20°–25° toward east (Lin et al., 2009; Liu et al., 2003). The Muchiliao Fault is a thrust fault and might have reactivated during Late Quaternary. However, it may be a blind fault due to the lack of outcrops. The Liuchia Fault is a thrust fault and cuts across Holocene sediments.

The Tachienshan Fault is located on the border of the Western Foothills: it can be divided into two segments. The NE-striking northern segment reactivated in the 1999 Chi–Chi earthquake with both reverse and right-lateral movement. The strike of southern segment changes from NE–SW to NW–SE with only reverse-slip component. The Chukou Fault trends NE–SW and separates imbricate faults in the eastern mountainous region from the distributed hills, tablelands, and alluvial plains to the west.

In this study, we assume that the Jiuchiunken Fault, the Muchiliao Fault, and the Liuchia Fault belong to the same fault system. These three faults have a similar trend of NNE and are all located along the boundary between the Coastal Plain and Western Foothills. The Tachienshan Fault and Chukou Fault can be considered as another fault system. In the Coastal Plain, seismic reflection data suggests the existence of a blind fault, the Chiayi Fault (Fig. 1) (Chen et al., 2006; Yang, 2007; Yeh et al., 1999).

3. GPS data processing and analysis

A dense GPS array composed of 46 continuous GPS (CGPS) stations and 73 survey-mode sites have been constructed since 1993. The 46 CGPS stations are operated by several agencies, including the Institute of Earth Sciences, Academia Sinica (IESAS), Central Weather Bureau (CWB), Central Geological Survey (CGS), and Ministry of the Interior (MOI) since 1990. For all continuous GPS data, we choose the time interval from 2000 to 2007 to avoid the influence of 1999 Chi–Chi earthquake (M_w 7.6). More than half of the CGPS sites have been operated longer than 4 years, including 15 stations with a data period of about 8 years. About 30 survey-mode sites have been surveyed annually since 1993 and others have at least 5 measurements in more than 3 years (Table 1). The survey-mode GPS data are processed by Bernese software v.4.2 (Hugentobler et al., 2001), while the continuous GPS data are processed by GAMIT/GLOBK v.10.3 (Herring et al., 2006a,b) with standard procedures using double-difference observables and precise orbits. All available GPS data from 1993 to 2007 for each site are combined to form GPS position time series.

The velocity of each CGPS site is estimated from position time series through a model by removing outliers and systematic errors. The model includes linear rate, annual and semi-annual periodic motions, post-seismic relaxation, and offsets caused by coseismic jumps and instrument changes. We consider noise characteristics in GPS position time series to be time-dependent, meaning that the noises are not white noises (Johnson, 1995). By stacking the power spectral densities from residuals, we are able to estimate the spectral index to distinguish the characteristic of noises (Tsai, 2004; Tsai et al., 2007). The spectra indexes in east, north, and vertical components of CGPS data are −0.61, −0.62, and −0.55, respectively, implying that the noises are best described as a combination of white noise and flicker noise (Mao et al., 1999; Nikolaidis, 2002; Williams, 2003; Zhang et al., 1997). A more realistic noise model can give a better estimate of full covariance matrix and model parameters in GPS position time series (Fig. 2). The mean root-mean-square (RMS) values of residuals are 5.4 mm, 4.2 mm, and 11.2 mm in the east, north and up components, respectively. The common errors are removed by stacking 19 continuous GPS sites with the data period longer than 5 years. By removing the common errors, the precision of GPS data has been further improved. After a common-error correction, the standard errors of 46 CGPS stations in the Chiayi–Tainan area decrease to the values of 2.3 mm, 1.8 mm, and 7.2 mm in the east, north and up components, respectively (Table 2).

On the other hand, the survey-mode GPS data have less data points and are not allowed to execute sophisticated analyses. We only remove coseismic displacements of the Chi–Chi earthquake, particularly for the stations located at the northern part of the Chiayi–Tainan area. To obtain interseismic velocity for each station, we estimate the coseismic displacements as well as velocities before and after the Chi–Chi earthquake separately using a linear regression (Fig. 3). The differences of velocities before and after the Chi–Chi main shock are mostly less than 3 mm/yr. After the corrections for coseismic offsets, the average linear rates are re-estimated. The velocities and pertinent data for all continuous and survey-mode GPS stations in the Chiayi–Tainan area are listed in Table 1.

4. GPS velocity field

Fig. 4 shows the horizontal and vertical velocity fields with respect to Paisha, Penghu station (located on the Chinese continental margin) from 1993 to 2007. Near the western flank of Central Range, velocities show W-WNW directed motions with rates of 33–44 mm/yr and decrease to 0–5 mm/yr near the coast (Fig. 4a). Remarkable subsidence of 31–59 mm/yr is observed in the Coastal Plain (Fig. 4b), probably due to ground water withdrawal. Significant uplift of 5–20 mm/yr is also found to the east of the JMLF (hanging wall side).

Two velocity profiles across the northern and southern parts of the study area are shown in Fig. 5a and b, respectively. The east components increase from west to east on both profiles. A significant velocity change of 15–20 mm/yr is detected across the zone between the JMLF and the Chukou Fault. The vertical components indicate that the JMLF is located at a boundary which separates the region of subsidence to the west from the region of uplift to the east. In contrast, the north components only reveal slight changes on both profiles, as the shortening is mostly E–W directed in the Chiayi–Tainan area.

5. Elastic dislocation model

To invert for fault geometries and slip rates from GPS velocities, we consider three different approaches: (1) a block model, (2) a buried dislocation model, and (3) a two-dimensional fault model. The block model consists of two blocks bounded by a major active fault. The observed interseismic deformation is the sum of the effects of block motion and strain accumulation. For the buried dislocation model, the interseismic deformation on the surface results from steady slip on a décollement underneath the fold–thrust belt in western Taiwan. In the two-dimensional fault model, we adopt the fault geometry constrained by the balanced geologic cross sections from Yang (2007). The interseismic strain accumulation across the Chiayi–Tainan area is represented by slip on buried dislocations.

We invert for the optimal fault geometry with a priori constraints from the seismicity, geological data, and seismic reflection data. The relationship of GPS-derived velocity (v)and the slip rate (*s*)on the fault can be expressed as:

$$w\begin{bmatrix}\nabla\\ 0\end{bmatrix} = w\begin{bmatrix}G(m)\\ \beta\nabla^2\end{bmatrix}s + \varepsilon \quad (1)$$

where m is related to the fault geometry parameters, including fault length, width, strike, dip, depth, and location; G is the Green's function associated with m and is computed by Okada's elastic half-space model (Okada, 1985); ε represents model residual; w indicates the weight equivalent to the inverse square root of data covariance matrix. ∇^2 is

Table 1
Velocities of continuous GPS stations in the Chiayi–Tainan area (w.r.t. Paisha, Penghu).

Site	Lon (°)	Lat (°)	V_h (mm/yr)	Azi (°)	V_u (mm/yr)	Data period (yr)	Data num.
Table 1a							
8118	120.5449	23.4647	13.5 ± 0.6	271	5.1 ± 1.8	2000.4–2007.9	1802
C001	120.6043	23.4197	27.9 ± 0.5	285	5.4 ± 1.4	2000.4–2007.8	1890
C002	120.5691	23.3635	27.2 ± 0.6	279	7.7 ± 1.6	2000.7–2008.0	2153
CHIA	120.4251	23.4977	7.3 ± 0.5	276	−0.8 ± 1.5	2000.0–2007.9	2182
CHKU	120.1063	23.0802	2.3 ± 0.6	270	−2.2 ± 1.5	2003.4–2008.0	1598
CHYI	120.1321	23.4525	2.5 ± 0.6	196	−31.0 ± 2.3	2004.1–2007.8	1270
CHYN	120.2827	23.3950	3.8 ± 0.5	275	−4.3 ± 1.8	2000.0–2008.0	2651
CWEN	120.4447	23.4748	9.5 ± 0.7	298	2.3 ± 1.8	2005.8–2007.9	745
DNAN	120.4399	23.6756	5.2 ± 0.7	308	−8.2 ± 2.7	2004.9–2007.9	950
DONS	120.1460	23.4624	2.4 ± 0.5	178	−10.7 ± 9.7	2000.0–2007.9	1990
GAIS	120.5825	23.0820	39.6 ± 0.9	276	13.7 ± 2.8	2000.0–2007.9	1997
GS04	120.4987	23.5933	6.5 ± 0.7	305	4.7 ± 1.6	2004.8–2007.9	788
GS05	120.5603	23.5689	14.3 ± 0.6	287	2.5 ± 1.8	2004.8–2007.9	1014
GS06	120.5461	23.4674	15.4 ± 0.8	281	5.1 ± 2.0	2004.8–2007.9	1023
GS07	120.6467	23.4847	20.0 ± 0.7	282	7.8 ± 2.2	2004.8–2007.9	942
GS17	120.5977	23.5629	17.2 ± 0.9	285	6.3 ± 2.2	2005.7–2007.9	705
GS18	120.4657	23.4867	8.9 ± 0.7	282	−0.5 ± 1.6	2005.7–2007.9	677
GUKN	120.5806	23.6479	8.9 ± 0.5	298	0.4 ± 1.5	2002.9–2007.9	1537
HOKN	120.1268	23.1901	1.4 ± 0.5	236	−10.4 ± 1.6	2000.0–2008.0	2652
ICHU	120.2713	23.3627	4.0 ± 0.6	266	−4.5 ± 1.8	2003.8–2007.9	1424
JHCI	120.5393	23.5155	13.4 ± 0.7	284	4.4 ± 1.6	2005.6–2007.8	798
JONP	120.5159	23.4247	15.5 ± 0.6	285	4.8 ± 1.8	2004.9–2008.0	1026
KULN	120.4989	23.3328	25.9 ± 0.6	278	6.9 ± 1.6	2000.0–2008.0	2222
MESN	120.8182	23.2656	32.9 ± 0.7	275	11.1 ± 2.7	2002.4–2008.0	1684
MINS	120.7128	23.2772	33.5 ± 0.7	277	7.6 ± 1.9	2002.3–2008.0	1832
NANK	120.2594	23.1032	6.4 ± 0.7	263	3.2 ± 1.6	2003.3–2007.9	1426
PAOL	120.6948	23.1104	40.7 ± 0.6	273	13.1 ± 1.8	2002.3–2008.0	1810
PEIM	120.1605	23.2956	4.7 ± 0.5	282	−13.1 ± 2.9	2004.3–2007.9	910
PKGM	120.2974	23.5816	3.3 ± 0.5	16	−28.6 ± 2.3	2000.0–2007.9	2721
S011	120.3314	23.2072	9.9 ± 0.6	298	0.2 ± 1.6	2000.0–2008.0	2718
S092	120.5204	23.1867	29.8 ± 0.6	277	5.8 ± 1.4	2000.0–2007.7	1912
S103	120.4671	23.5661	8.7 ± 0.5	299	1.1 ± 1.5	2000.0–2008.0	2776
SILN	120.6347	23.1657	28.5 ± 1.1	275	8.4 ± 1.5	2003.4–2008.0	1494
SJPU	120.4753	23.4268	9.2 ± 0.7	277	4.1 ± 1.4	2003.1–2008.0	1665
SSUN	120.3697	23.4159	9.0 ± 0.9	289	4.5 ± 4.0	2006.2–2007.9	563
SUAN	120.2853	23.4883	4.8 ± 0.6	286	5.0 ± 2.1	2002.9–2007.9	1522
TAPU	120.5612	23.2673	30.8 ± 0.7	283	4.9 ± 1.7	2003.4–2007.9	1341
TAYN	120.7561	23.1611	34.2 ± 1.1	284	8.3 ± 3.9	2005.7–2007.8	702
TUNS	120.3966	23.3194	9.7 ± 0.6	282	3.3 ± 1.8	2002.9–2007.9	1502
W021	120.5414	23.5374	13.2 ± 0.5	281	4.8 ± 1.8	2002.0–2008.0	2042
W029	120.6561	23.5426	24.8 ± 0.7	275	7.0 ± 1.5	2000.4–2008.0	2641
WANC	120.5182	23.1887	29.0 ± 0.6	280	6.0 ± 2.2	2004.3–2007.9	835
WANS	120.8771	23.6093	33.1 ± 0.7	292	10.7 ± 2.1	2005.3–2007.9	786
WUST	120.3715	23.1981	13.9 ± 0.8	277	6.8 ± 1.8	2003.1–2007.9	1391
YSAN	120.0779	23.1483	2.4 ± 0.6	235	−3.3 ± 1.8	2004.9–2007.9	1074
YUSN	120.9510	23.4891	44.0 ± 0.8	292	9.2 ± 1.9	2000.0–2007.9	2196
Table 1b							
0228	120.6000	23.5689	21.1 ± 1.9	283	4.6 ± 3.3	2001.5–2007.1	7
0437	120.4594	23.2388	18.4 ± 0.8	276	5.6 ± 0.8	1993.4–2007.1	14
7205	120.7574	23.0768	42.1 ± 0.9	270	10.9 ± 1.2	1993.4–2004.7	19
C004	120.5707	23.4491	16.2 ± 1.3	272	21.0 ± 4.0	2000.6–2007.1	13
C006	120.5285	23.0794	43.9 ± 1.4	271	0.3 ± 1.4	1996.1–2007.1	10
C008	120.5846	23.5632	18.2 ± 1.6	279	14.3 ± 3.4	2000.6–2007.1	9
C012	120.5688	23.5547	16.8 ± 1.7	279	20.2 ± 3.8	2000.6–2007.1	12
C013	120.5854	23.5257	18.8 ± 1.9	273	19.3 ± 5.6	2000.6–2007.1	9
G076	120.4796	23.6072	4.1 ± 2.2	273	−1.1 ± 4.5	2002.7–2007.1	9
G077	120.5468	23.6282	4.2 ± 2.4	288	6.2 ± 1.8	2002.7–2007.1	9
G082	120.2320	23.4618	4.1 ± 2.5	328	−27.8 ± 2.9	2000.0–2004.6	9
G086	120.4911	23.5099	10.7 ± 1.0	277	4.3 ± 1.1	2000.6–2007.1	12
G088	120.5524	23.5822	9.7 ± 2.1	292	8.2 ± 2.0	2002.7–2007.1	8
G105	120.4478	23.4612	10.5 ± 1.4	278	−0.8 ± 2.2	2000.6–2007.1	9
G106	120.3225	23.4572	4.3 ± 0.9	282	−5.4 ± 2.8	2000.6–2007.1	10
G107	120.5477	23.4673	15.6 ± 1.9	275	7.1 ± 2.5	2000.6–2007.1	9
G110	120.3880	23.4298	7.9 ± 1.3	285	2.1 ± 5.5	2000.6–2007.1	9
G111	120.5038	23.4051	13.7 ± 1.4	278	−2.6 ± 1.6	2000.6–2007.1	15
G115	120.4060	23.3548	8.5 ± 1.1	277	−11.7 ± 2.4	2000.6–2007.1	17
G116	120.4597	23.3861	10.9 ± 0.9	280	−2.9 ± 2.2	2000.6–2007.1	14
G119	120.1927	23.2897	3.7 ± 0.7	315	−35.9 ± 2.7	2001.6–2007.1	8
G122	120.2645	23.2520	6.4 ± 0.9	289	−22.8 ± 2.4	2000.6–2007.1	12
G125	120.1669	23.2398	2.9 ± 1.9	325	−30.5 ± 3.2	2000.6–2007.1	9
G129	120.2458	23.1886	9.4 ± 2.1	275	−9.7 ± 0.8	1999.0–2007.1	6
G132	120.0903	23.0956	4.2 ± 1.2	260	−5.9 ± 1.7	1999.0–2007.1	6

Table 1 (*continued*)

Site	Lon (°)	Lat (°)	V_h (mm/yr)	Azi (°)	V_u (mm/yr)	Data period (yr)	Data num.
Table 1b							
G135	120.2804	23.1373	8.3 ± 1.3	262	−2.9 ± 2.1	1999.0–2007.1	7
G137	120.4098	23.1497	16.3 ± 0.9	278	13.5 ± 1.7	1999.0–2007.1	9
G138	120.4502	23.1218	29.7 ± 1.3	275	2.8 ± 1.1	1999.0–2007.1	8
G336	120.4737	23.4856	8.7 ± 2.6	267	0.0 ± 2.9	2002.8–2007.1	8
G337	120.5503	23.4866	13.5 ± 2.6	272	7.9 ± 5.1	2002.8–2007.1	7
G338	120.4189	23.4974	8.0 ± 1.9	292	0.2 ± 5.7	2002.8–2007.1	7
G345	120.4480	23.5360	7.5 ± 2.6	272	8.2 ± 3.8	2002.8–2007.1	5
G459	120.3536	23.1214	6.5 ± 2.1	261	7.8 ± 2.4	2003.6–2007.1	5
G848	120.4655	23.3454	18.7 ± 4.8	286	−1.5 ± 1.8	2003.6–2007.1	7
G854	120.4965	23.4921	5.2 ± 2.0	261	−11.9 ± 12.0	2003.6–2007.1	6
G856	120.6122	23.4765	17.7 ± 4.3	273	3.1 ± 2.3	2003.6–2007.1	5
G862	120.6620	23.4741	23.9 ± 3.2	286	9.7 ± 6.9	2003.6–2007.1	5
GB15	120.4285	23.3472	9.1 ± 1.5	284	−3.0 ± 2.3	2004.6–2007.1	5
M093	120.4629	23.6955	0.8 ± 0.8	83	−16.8 ± 1.9	2000.0–2006.9	12
S003	120.1546	23.1749	1.7 ± 0.4	287	−17.0 ± 0.9	1993.4–2007.1	19
S004	120.1806	23.3843	2.2 ± 0.4	286	−44.2 ± 2.0	1993.4–2007.1	15
S005	120.2085	23.6009	3.4 ± 0.6	80	−48.5 ± 1.2	1993.4–2007.1	14
S007	120.3751	23.2558	11.5 ± 0.6	273	0.9 ± 0.7	1993.4–2007.1	16
S008	120.4355	23.4218	10.5 ± 0.3	278	0.3 ± 0.6	1993.4–2007.1	14
S013	120.5556	23.2554	26.9 ± 0.5	280	2.0 ± 0.8	1993.4–2007.1	14
S014	120.6406	23.4062	21.0 ± 0.4	271	5.5 ± 0.3	1993.4–2007.1	16
S015	120.6733	23.5568	19.8 ± 0.7	280	2.4 ± 0.4	1993.4–2007.1	16
S025	120.8163	23.2654	33.2 ± 0.9	274	9.0 ± 1.6	1993.4–2003.6	11
S026	120.9082	23.2840	36.8 ± 1.1	283	7.2 ± 1.4	1993.4–2003.9	14
S027	120.8814	23.4856	33.0 ± 1.0	288	4.8 ± 1.0	1993.4–2006.1	21
S065	120.6030	23.1216	37.5 ± 0.9	274	10.7 ± 2.8	1993.4–2002.5	12
S066	120.5036	23.1941	29.0 ± 0.5	276	1.4 ± 1.1	1993.4–2007.1	14
S068	120.3583	23.0869	9.7 ± 1.1	267	5.4 ± 1.0	1996.1–2007.1	12
S069	120.4930	23.3282	24.8 ± 0.7	274	6.0 ± 1.0	1993.4–2003.6	10
S070	120.5540	23.4538	14.8 ± 0.6	278	−4.8 ± 1.3	1993.4–2007.1	17
S071	120.3139	23.4711	3.0 ± 0.6	314	2.6 ± 0.6	1993.4–2007.1	13
S082	120.3606	23.2370	9.8 ± 0.5	270	−3.0 ± 0.6	1994.1–2007.1	12
S083	120.3810	23.2384	15.1 ± 0.6	265	9.2 ± 1.4	1993.4–2007.1	14
S085	120.4073	23.2373	16.3 ± 0.5	266	4.4 ± 1.1	1993.4–2007.1	13
S086	120.4209	23.2441	18.5 ± 0.7	275	14.3 ± 1.2	1993.4–2005.5	10
S087	120.4404	23.2377	15.3 ± 0.6	279	6.9 ± 1.3	1993.4–2007.1	13
S088	120.4512	23.2421	17.7 ± 0.7	277	5.9 ± 1.0	1993.4–2007.1	15
S089	120.4594	23.2230	19.1 ± 0.4	274	6.0 ± 1.0	1993.4–2007.1	14
S090	120.4725	23.2111	23.6 ± 0.4	267	10.2 ± 1.0	1993.4–2007.1	14
S091	120.4861	23.2064	29.4 ± 0.6	277	4.6 ± 1.7	1993.4–2007.1	12
S094	120.4934	23.6625	2.5 ± 0.3	279	−7.3 ± 0.7	1993.4–2007.1	26
S291	120.3044	23.3400	7.2 ± 0.5	260	−17.4 ± 1.0	1995.3–2007.1	13
S421	120.5957	23.4608	17.1 ± 1.3	273	23.6 ± 3.0	1998.6–2007.1	15
S901	120.3530	23.5973	7.8 ± 0.9	312	−59.0 ± 1.9	1997.1–2007.1	11
S906	120.2034	23.1208	5.1 ± 0.9	257	−8.4 ± 2.0	1998.0–2007.1	9
SINS	120.2926	23.0862	9.3 ± 1.0	260	−3.1 ± 1.5	2000.1–2007.1	8
STCS	120.4727	23.5376	8.3 ± 0.4	285	3.6 ± 0.6	1993.4–2006.1	12
TJSN	120.6150	23.5918	25.7 ± 1.3	272	9.2 ± 1.8	1998.6–2007.1	8

Note: Lon and Lat are the longitude and latitude of GPS sites, respectively. V_h and V_u are the horizontal and vertical components of station velocities with standard errors, respectively and Azi is the azimuth of the horizontal velocity. Data period shows the start and end time of observation period. Data Num. is the total number of data points.

the Laplacian operator used to constrain the smoothness of fault slip rate. β is a parameter determining the weight between the model roughness versus data misfit, and is obtained by cross-validation (Matthews and Segall, 1993).

The fit to GPS observations is quantified by the mean value of normalized square residuals, χ^2, and is expressed as

$$\chi^2 = \frac{1}{N-7}\left\|\sum^{-1/2}(G(m)s-\nabla)\right\|^2 \quad (2)$$

N is the number of data points, 7 is the number of model parameters, $\sum^{-1/2}$ is the inverse square root of data covariance matrix. When $\chi^2 = 1$, it means that the model fits the data within uncertainty on average.

In all models, we estimate optimal fault parameters using a grid search, and compute 95% confidence interval for each model parameter using a bootstrap method.

5.1. Block model

The interseismic deformation is modeled as the sum of a steady rigid block motion and a negative dislocation (back slip) on the fault (Matsu'ura et al., 1986; Savage, 1983). The back-slip rates are the slip-rate deficits on the fault which are presumably to be released in forthcoming earthquakes.

Large earthquakes have occurred on some of these faults (Cheng and Yeh, 2005); for example, the 1906 Meishan earthquake (M_L 7.1) and the 1946 Hsinhua earthquake (M_L 6.1) which are related to the Meishan Fault and Hsinhua Fault, respectively. The GPS data between 1993 and 2007 indicate that the difference in velocity across the Meishan Fault is only about 3–5 mm/yr (estimated from 7 near-field sites including G007, G076, and GS04 on the footwall and G088, G345, S103 and STCS on the hanging wall). Note that the Hsinhua Fault is located near the southern termination of the study area. We do not attempt to model the strain accumulation on this fault.

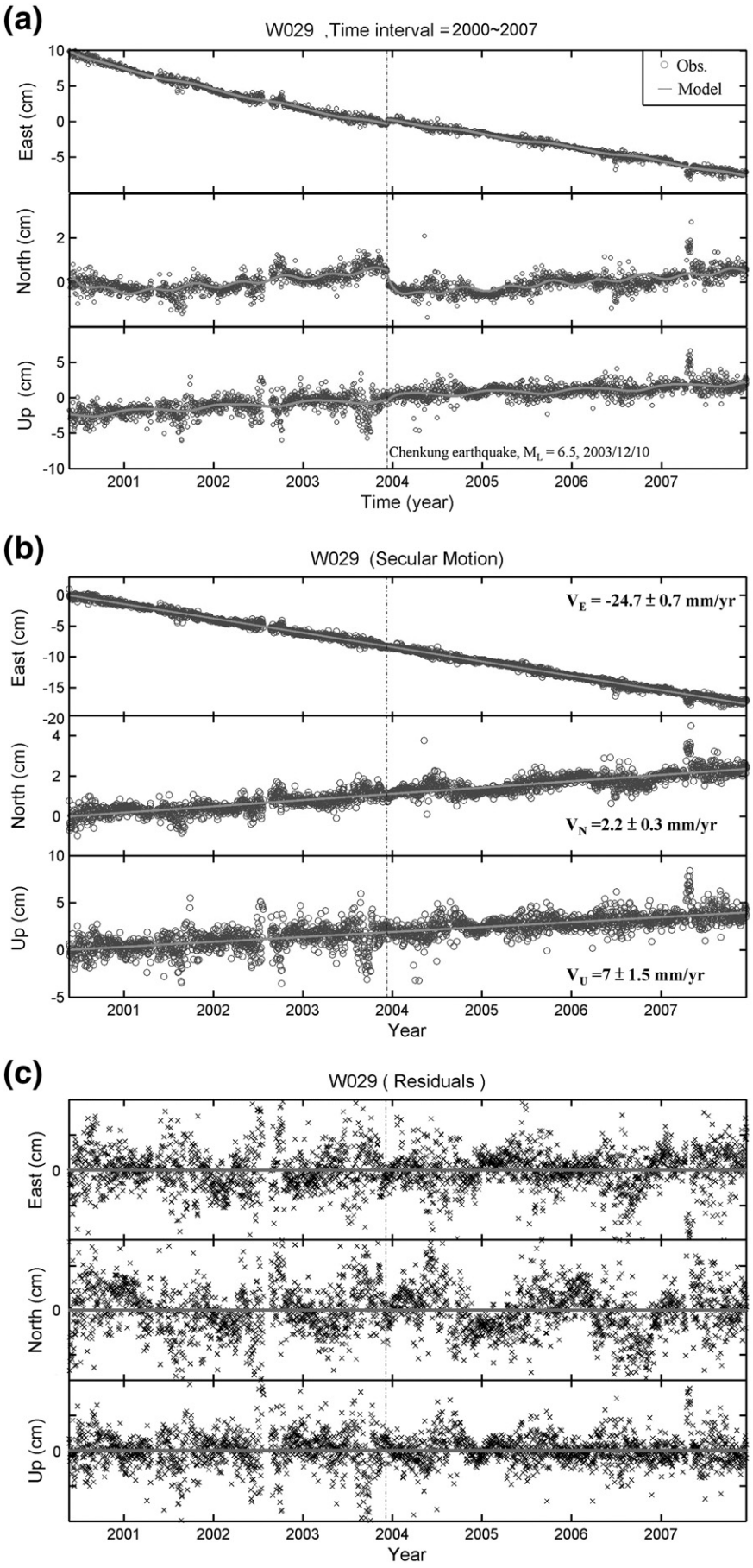
(a)
W029 ,Time interval =2000~2007
Obs.
Model
East (cm)
North (cm)
Up (cm)
Chenkung earthquake, M_L = 6.5, 2003/12/10
Time (year)
(b)
W029 (Secular Motion)
V_E = -24.7 ± 0.7 mm/yr
V_N =2.2 ± 0.3 mm/yr
V_U =7 ± 1.5 mm/yr
Year
(c)
W029 (Residuals)
Year

Table 2
The data precision, common error, and RMS values of residuals for 46 continuous GPS stations in the Chiayi–Tainan area.

Sites	RMS (mm/yr)		
	R_E	R_N	R_U
8118	3.1	2.0	9.3
C001	2.6	2.0	8.0
C002	2.1	1.7	6.1
CHIA	1.8	1.7	6.0
CHKU	1.7	1.6	5.1
CHYI	2.1	1.4	7.2
CHYN	2.5	1.7	8.7
CWEN	1.6	1.5	5.4
DNAN	1.7	1.5	6.8
DONS	2.6	1.5	29.1
GAIS	4.2	3.3	11.5
GS04	1.7	1.5	6.0
GS05	1.6	1.3	5.1
GS06	1.8	1.3	5.4
GS07	1.6	1.5	6.4
GS17	1.5	1.5	5.4
GS18	1.4	1.1	4.7
GUKN	1.7	1.7	5.7
HOKN	1.8	1.6	6.5
ICHU	1.6	1.5	5.7
JHCI	1.7	1.4	5.7
JONP	1.5	1.2	5.6
KULN	2.7	1.4	5.9
MESN	2.8	2.0	9.4
MINS	2.3	2.1	7.5
NANK	1.7	1.9	5.6
PAOL	2.5	2.0	7.3
PEIM	1.9	1.5	9.7
PKGM	2.0	1.6	8.9
S011	3.1	3.2	6.1
S092	4.7	2.4	7.1
S103	2.0	1.5	5.3
SILN	5.3	3.1	6.5
SJPU	2.0	2.4	5.4
SSUN	1.7	1.3	5.1
SUAN	1.7	1.4	6.5
TAPU	2.1	2.0	7.0
TAYN	2.4	2.0	8.2
TUNS	1.7	1.4	5.8
W021	2.2	1.7	6.2
W029	1.9	1.8	6.4
WANC	2.2	1.8	6.7
WANS	2.6	1.7	7.5
WUST	3.8	1.4	5.3
YSAN	1.9	1.8	6.1
YUSN	4.8	3.5	10.6
P_{cgps}	2.3	1.8	7.2
E_{com}	2.1	1.5	6.6

Note: R_E, R_N, and R_U represent the RMS values of residuals without common error for 46 continuous GPS stations in the east, north and up components, respectively. P_{cgps} is the mean value of R_E, R_N, and R_U for 46 continuous GPS stations; it represents the precision of continuous GPS data without common errors. E_{com} is the common error by stacking 19 continuous GPS sites with data period longer than 5 years.

There is no clear evidence showing activity along the Chukou Fault (Shyn and Sieh, 2005). In contrast, some geomorphic evidence of youth deformation exists further west of Chiayi Hills, near the Jiuchiunken–Muchiliao–Liuchia Fault zone. Uplifted Late Quaternary lateritic fluvial terraces in the Chiayi Hills west of Chukou Fault and Coastal Plain clearly indicate deformation across several folds and minor faults (Chen, 1999; Huang, 1996; Hung et al., 1999). These lines of evidence indicate present major active faults are located below Chiayi Hills and Chianan Coastal Plain. Thus, we conduct a block model consisting of two blocks bounded by a major fault system, Jiuchiunken–Muchiliao–Liuchia Faults (JMLF), to study the interseismic deformation. To avoid the effect of non-tectonic signals and obtain a more reliable result, we remove vertical data which falls into the following three categories: (1) the data period less than 5 years for survey-mode sites; (2) the number of surveys less than 5 times; (3) the subsidence rate larger than 5 mm/yr affected by the ground water withdrawal. We end up using vertical data from 61 GPS sites which are mostly located on the hanging wall of the JMLF.

We divide the fault into small rectangle patches with the size of about 8×8 km^2 and use GPS horizontal velocities of 119 sites and vertical velocities of 61 sites to invert for fault parameters. In our model, the velocity of the western block is fixed to 0. We use a grid search method to find optimal fault parameters and a bootstrap method to obtain the 95% confidence interval of each parameter (Table 3a). The inferred velocity of the eastern block (Block 2) is 42 mm/yr in the direction of 280° with a 95% confidence interval of 39–46 mm/yr in rate and 274°–286° in azimuth with respect to the western block (Block 1). The maximum back-slip rate of 38 mm/yr near the JMLF is very close to the long-term slip rate (42 mm/yr). This feature suggests that the JMLF is nearly fully locked. The optimal dip and locking depth are 23° and 13 km, respectively. Fig. 6 shows the comparison between model predictions and GPS observations and inferred fault-slip distribution. Most model parameters are well constrained by GPS data. The optimal model can explain about 90% of data variance.

We also take the Chiayi Fault to be the block boundary for another modeling study. However, the result of inversion is divergent. It is difficult to find optimal model parameters. Since the model resolution is affected by the station spatial coverage, the scarcity of stations near the Chiayi Fault may lead to a poor resolution on model parameters.

5.2. Buried dislocation model

Previously studies in the Chiayi–Tainan area suggest that frontal thrusts in western Taiwan sole into a single décollement at depths (Huang et al., 1995; Suppe, 1976, 1980). We assume that the observed GPS velocities result from uniform steady slip on the subsurface décollement and the frontal thrust faults are locked in the interseismic period. We use a rectangular décollement with the strike of 21° approximately parallel to the JMLF system. We invert for fault parameters including the locking depth, dip, and location of the décollement.

The optimal model parameters and their 95% confidence intervals are listed in Table 3b. The optimal buried dislocation model explains about 90% of data variance with a uniform slip rate on the décollement of 41.6 mm/yr in the direction of 275° and a fault depth of 8 km with a 95% confidence interval of 5–12 km (Fig. 7). The vertical projection of the western edge of décollement to the surface is located to the east of the Chukou Fault. Additionally, we find the horizontal position and the depth of the western edge of the décollement are highly correlated. The depth of décollement becomes deeper when the western edge of décollement moves further east. If we assume the future fault rupture extends from the top edge of décollement to the surface trace of JMLF, the dip angle of this fault is about 22° (Fig. 7). The fault geometry is consistent with the result of the block model which gives the optimal fault dip of 23°, fault depth of 13 km and block velocity of 42 mm/yr.

5.3. Two-dimensional fault models

In the previous section, we find the block model can roughly constrain the subsurface fault geometry of the Jiuchiunken–Muchiliao–Liuchia Fault system, while it fails to resolve the geometry and slip rate of the

Fig. 2. GPS position time series from a continuous GPS station, W029. The dash line denotes the occurrence time of 2003 Chenkung earthquake (M_L 6.5). (a) Position time series in east, north, and vertical components. The circles indicate GPS daily solutions and solid lines indicate the model predictions. (b) The position time series of station W029 after removing coseismic, postseismic and periodic motions. The solid line indicates the estimated interseismic velocity. (c) The residuals of east, north, and vertical components after conducting time series analysis. The solid lines denote linear regression of residuals. The slopes are nearly zero indicating the position time series of W029 is well-corrected.

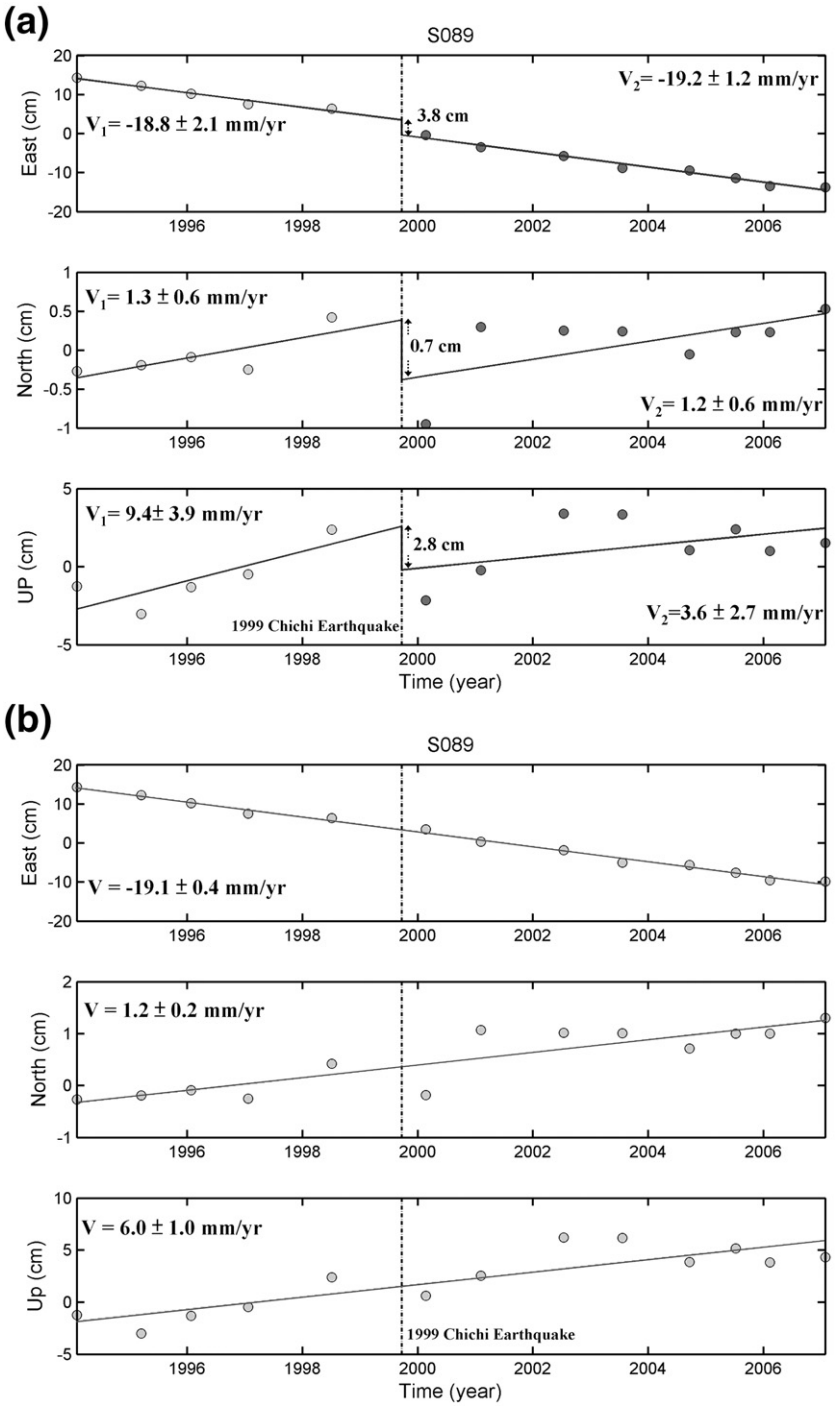

Fig. 3. GPS position time series of a selected survey-mode GPS site, S089. The dash line denotes the occurrence time of 1999 Chi–Chi earthquake. (a) The white and gray circles show data before and after Chi–Chi earthquake, respectively. A linear regression is used to obtain the velocities before and after earthquake in the east, north, and vertical components. The vertical lines mark coseismic offsets. (b) GPS position time series after the correction of coseismic offsets. The solid lines show interseismic velocity estimated by a linear regression.

Chiayi Fault. Here we propose two 2D fault models constructed from balanced geologic cross sections by Yang (2007) (Fig. 1). In a 2D model, the interseismic strain accumulation across the Chiayi–Tainan area is represented by slip on buried dislocations. In the northern profile, the Chiayi Fault is a blind thrust fault with the fault tip at the depth of 1–2 km and dip 25° toward the east. The Chiayi Fault merges into the Jiuchiunken Fault and Chukou Fault at 6 km depth. The dips of Jiuchiunken Fault and Chukou Fault are 26°E and 32°E, respectively. These frontal thrust faults connect to the sloping décollement at 10 km depth with the dip of about 17°E. In the southern profile, the Chiayi Fault is a blind fault with the fault tip at depth of 2 km and dip of 20°E. The Chiayi Fault merges with the Liuchia Fault (the southern part of the JMLF system) and Chukou Fault at depths and connects to the sub-horizontal décollement (dip 6°E) at a depth of 9 km.

We use 51 and 46 GPS sites on the northern and southern profiles, respectively (Fig. 8a) and project the observed horizontal velocities to the directions perpendicular to the fault strikes, 10° and 21.6° in northern and southern profiles, respectively. Fig. 9 shows our model

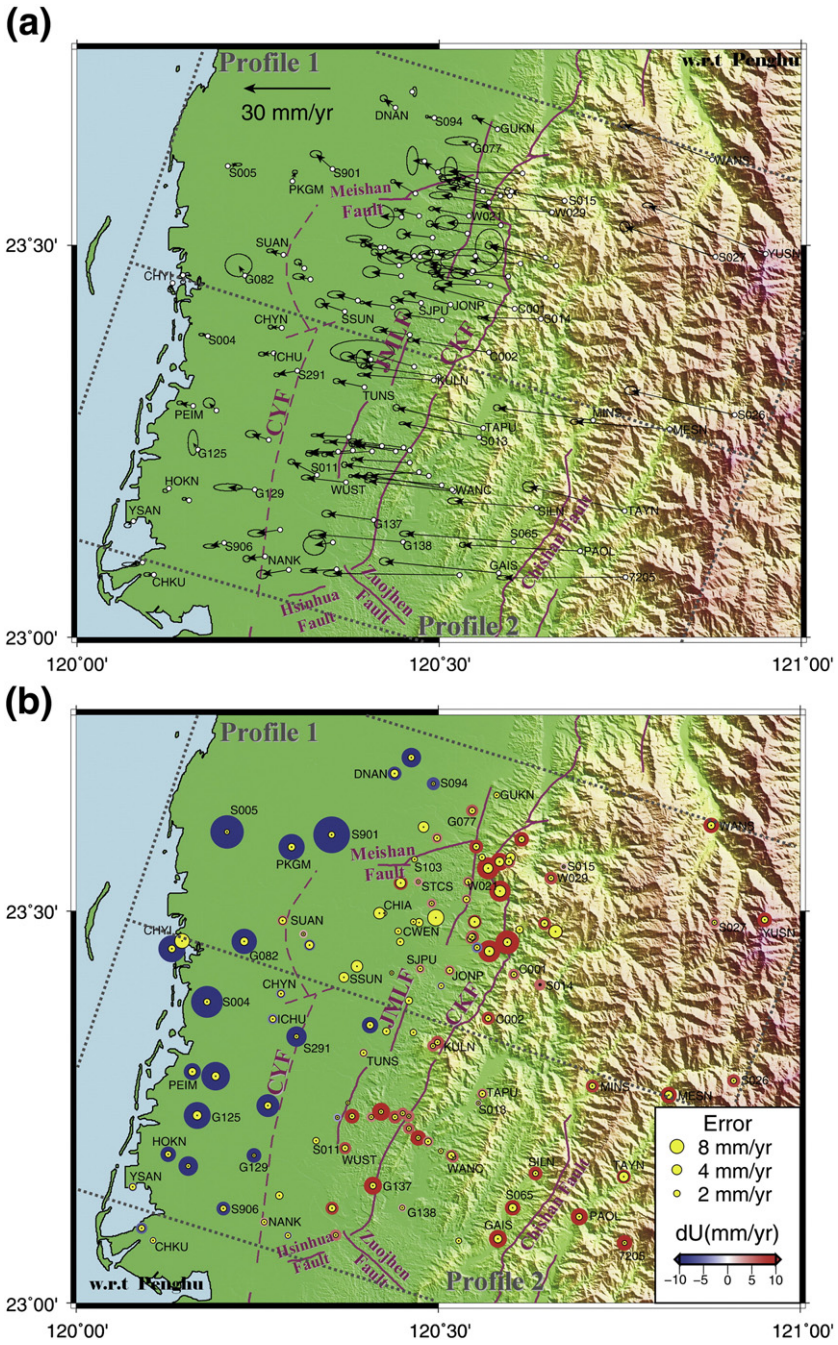

Fig. 4. GPS velocity field from 1993 to 2007. The magenta lines indicate the surface traces of faults. CYF, JMLF, and CKF denote the Chiayi Fault, Jiuchiunken–Muchiliao–Liuchia Fault system and Chukou Fault, respectively. (a) Horizontal velocity (black vectors) with respect to S01R, located at Penghu. A 95% confidence error ellipse is shown at the tip of each velocity vector. The gray dashed rectangles show regions for plotting two velocity profiles in Fig. 5. (b) The vertical GPS velocity with respect to S01R. The size of circle is proportional to the vertical motion. Blue circles denote subsidence and red circles denote uplift. The yellow circles are standard deviations.

fault geometries for northern and southern profiles which are very close to the proposed geometries constrained by the balanced geologic cross sections of Yang (2007). In the northern profile, 8 sub-faults are used to model the subsurface fault geometry (Fig. 9a). Sub-faults 1, 3, and 5 represent the frontal thrust faults: Chiayi Fault (CYF), JMLF, and Chukou Fault (CKF), respectively, while the sub-fault 8 is the décollement. Other sub-faults (2, 4, 6, and 7) are used to connect the décollement with the frontal thrust faults. A similar approached, with 10 sub-faults, is adopted to construct the geological structures in the southern profile. The sub-fault 10 denotes the décollement and the CYF, JMLF, and CKF are modeled by sub-faults 1, 3, and 7, respectively. The tip lines of the CYF, JMLF, and CKF are fixed. To avoid the boundary effect, we use a very large fault length for each sub-fault and a large fault width for the décollement. We then invert for both fault slip rates and perturbations from our initial geometry using a grid search approach to obtain an optimal set of fault parameters (Table 4). The 95% confidence intervals of fault parameters are given by using a bootstrap method.

Fig. 10 shows the observed and model predicted velocity components for the northern and southern profiles. V_h and V_u denote horizontal and vertical velocity components, respectively. In general, the

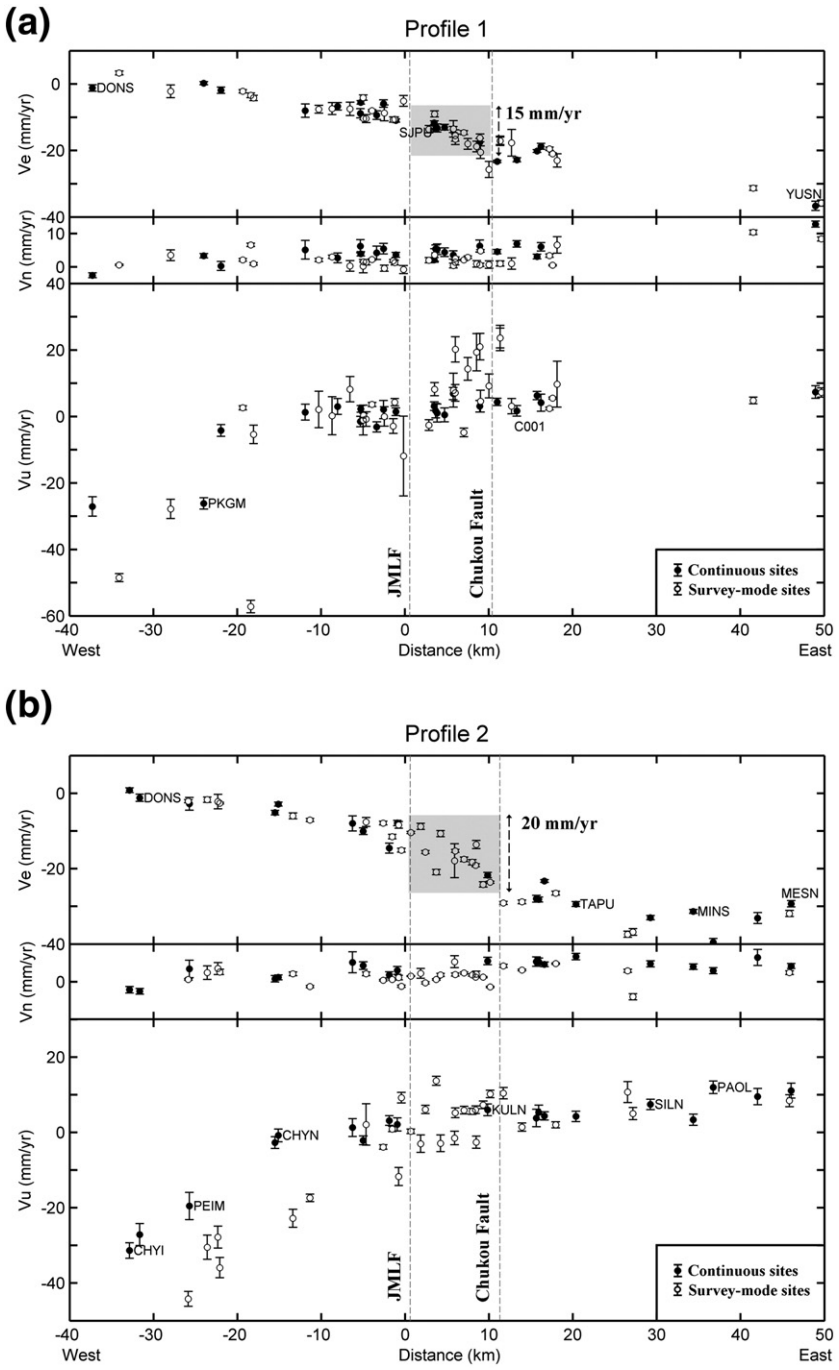

Fig. 5. Velocity profiles in northern and southern part of the Chiayi–Tainan area. The profile locations are shown in Fig. 4. The dash lines indicate the locations of JMLF and Chukou Fault. The solid dots and circles with error bars denote the east, north, and up velocity components and their uncertainties for continuous and survey-mode sites, respectively. (a) Profile 1, velocity profile in the northern part of the Chiayi–Tainan area. The light-gray rectangular region denotes a velocity change of about 15 mm/yr in east component across the JMLF and Chukou Fault. (b) Profile 2, velocity profile in the southern part of the Chiayi–Tainan area. The light-gray rectangular region denotes a velocity change of about 20 mm/yr in east component across the JMLF and Chukou Fault.

model fits the observed data very well. The inferred dip of CYF, JMLF, and CKF are 20°, 25°, and 28° with 95% confidence intervals of 17°–22°, 21°–28°, 22°–31°, respectively, in the northern profile (Table 4). There is almost no slip at shallow depths of the JMLF and the CKF which extend to the ground surface. The optimal dip and depth of western edge for décollement are 5° and 10 km with 95% confidence intervals of 0°–9° and 8–13 km, respectively. Comparing with the results from balanced geologic cross sections of Yang (2007), the depth of décollement is essentially the same, but the dip angle is sub-horizontal. The slip rate on the décollement is 46 mm/yr. In the southern profile, the CYF, JMLF and CKF are sole into the 7° east-dipping décollement at a depth of 10 km. The 95% confidence intervals for the depth and dip of décollement are 11–13 km and 4°–10°, respectively. The inferred slip rate is about 44 mm/yr on the décollement. The dip angles of the CYF, JMLF and CKF are 20°, 30°, and 24° with 95% confidence intervals of 18°–22°, 25°–32°, and 20°–27°, respectively (Table 4). The optimal models for northern and southern profiles indicate that the CYF does not extend to the surface and terminates at a

Table 3
(a) The optimal model parameters for block model. The block boundary is the JMLF system. (b) The optimal parameters of buried dislocation model. The optimal values and their 95% confident interval for each model parameter are listed.

		optimal	95% confi.	Residual (mm/yr)	Wrms (mm/yr)	χ^2	Rvar (%)
(a) Block model							
Block	V2 (mm/yr)	42	39–46	3.6	2.5	5.7	90%
	Dir2 (°)	280	274–286				
Fault	Dip (°)	23	19–27				
	Depth (km)	13	10–17				
(b) Buried dislocation model							
Fault	Dip (°)	0	0–7	4.1	2.8	7.8	90%
	Depth (km)	8	5–12				

Note: Wrms is the model weighted root mean square value; residual is the average of model residuals; χ^2 is the chi-square value, a mean value of normalized square residuals; and Rvar is the explainable variance.

depth of 1 km. Furthermore, the interseismic slip rates on the frontal thrust faults are all less than 4 mm/yr, much smaller than slip rates of 44–46 mm/yr on the décollement. This implies the shallow portions of faults are almost fully locked in the interseismic period.

6. Discussion

Fig. 8a shows the seismicity with magnitude (M_L) larger than 3 in the Chiayi–Tainan area between 1992 and 2007. High seismic activity surrounding the Peikang Basement High is prominent. Basically, the earthquakes distribute in a wide area and it is difficult to ascertain the connection between earthquake locations and fault geometries (Hsu et al., 2008). Based on the seismicity from 1992 to 2007, we plot two seismicity profiles with the optimal fault geometry from our 2D fault modeling results (Fig. 8b). In the northern profile, almost no earthquake happened at shallow depths on the CYF, JMLF, and CKF wherein small slip rates of less than 2 mm/yr are derived. Most earthquakes occur below and near the western edge of the décollement. There are more shallow earthquakes in the southern profile compared to those in the north. The seismicity at 10 km depth wherein frontal thrust faults connect to the décollement seems to be more active compared to adjacent regions.

Fig. 11 gives a summary of optimal fault parameters for four models obtained in this study. The block modeling result shows that the long-term slip rate (block velocity) is 42 mm/yr in the direction of 280° to the east of the JMLF system, corresponding to the azimuth of maximum compressional stress axes (100°/280°) inferred from fault-slip

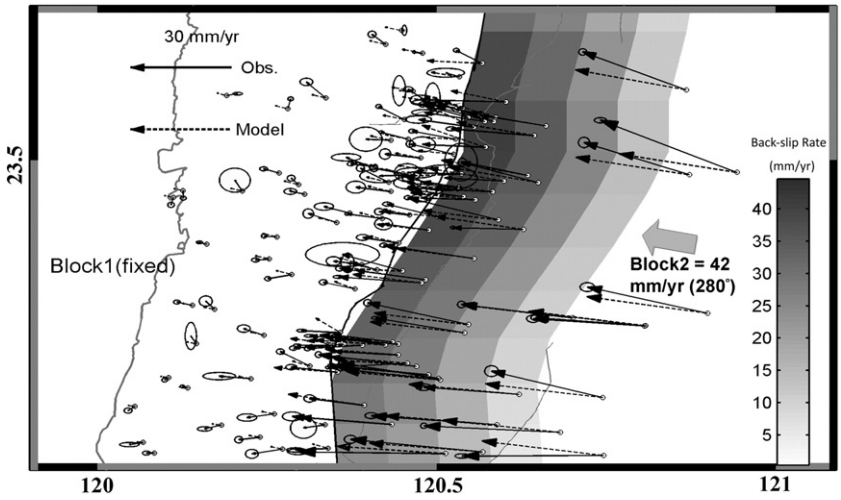

Fig. 6. The observed (black vectors) and model predicted (dashed vectors) interseismic velocities from a two-block model. A 95% confidence error ellipse is shown at the tip of each observed velocity vector. The large gray arrow represents the block motion of Block 2. The surface projection of back-slip distribution is also shown in gray scale.

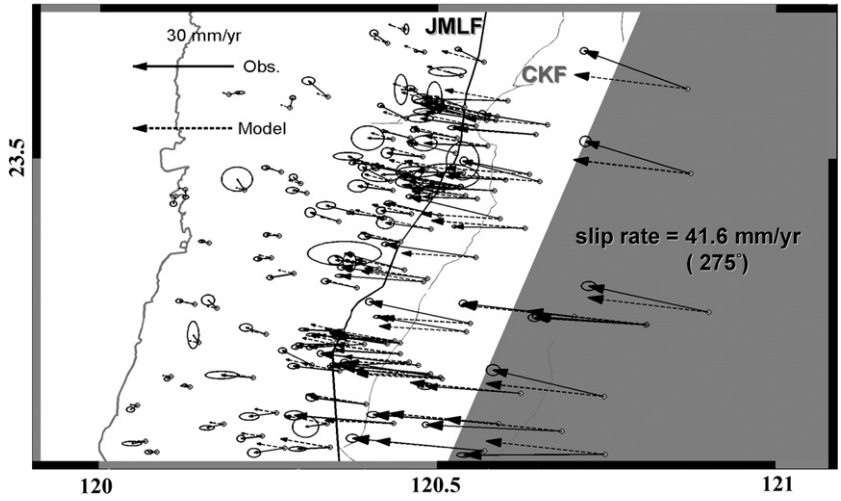

Fig. 7. The observed (black vectors) and model predicted (dashed vectors) interseismic velocities for a buried dislocation model. A 95% confidence error ellipse is shown at the tip of each observed velocity vector. The optimal buried dislocation model result indicates the uniform slip rate on the décollement is 41.6 mm/yr in the direction of 275°, which is similar to the block motion (42 mm/yr, in 280°) from the block modeling result.

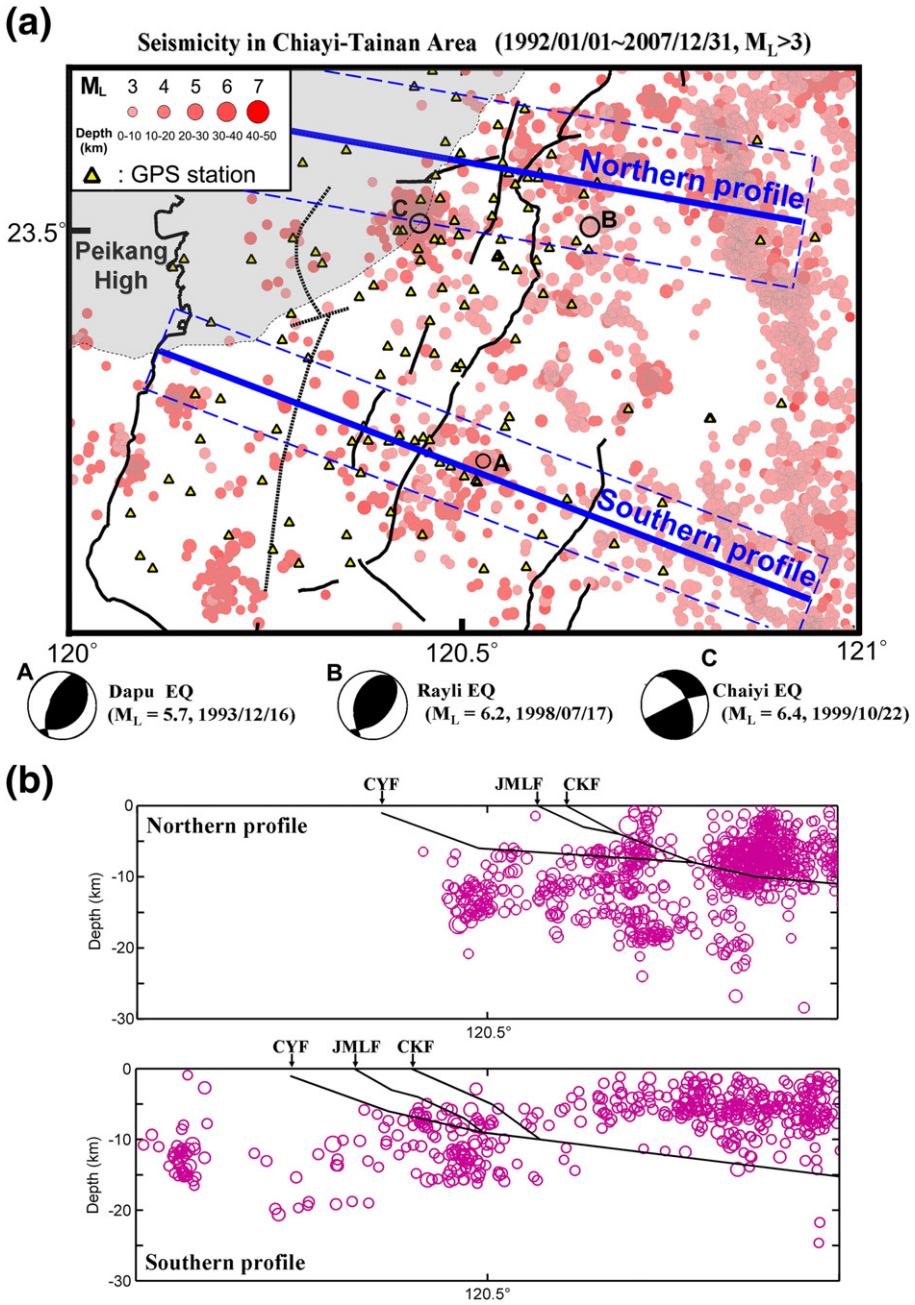

Fig. 8. The seismicity and two cross-sections of hypocenters in the Chiayi–Tainan area. (a) Seismicity from 1992 to 2007 with $M_L > 3$ and depth less than 50 km. Circles indicate the epicenters with circle size proportional to magnitude. The locations of major active faults and 3 disastrous earthquakes occurred since 1992 in the Chiayi–Tainan area are also shown. These earthquakes are denoted by characters A, B, and C. The two blue lines indicate the locations of cross-sections for 2D fault models and hypocenters. Triangles indicate location of GPS stations. (b) The illustration of two-dimensional fault models and seismicity in the northern and southern profiles.

directions and the paleo-stress field in the Western Foothills (Angelier et al., 1986). This result is also consistent with the study of paleomagnetic data which indicates the average direction of paleo-stress is about 100°–110° (Lee and Angelier, 1995). On the other hand, our buried dislocation model indicates that the existence of a horizontal décollement at a depth of 8 km with a uniform slip rate of 41.6 mm/yr in agreement with long term slip rate of 42 mm/yr from the block model and the slip rate of 40 mm/yr on the décollement from a 2D buried dislocation model (Hsu et al., 2003). The block model (11a) suggests that the most likely scenario of future earthquake might occur on the JMLF. In reality, most thrust faults rooted into décollement in western Taiwan and interseismic deformation has no resolution of which frontal thrust would break in the future since these faults are mostly fully locked. There is still a possibility that earthquakes may occur on other frontal thrusts as inferred from the buried dislocation model that accumulated strain would be released to any fault located to the west edge of the décollement.

We also construct 2D fault models taking account of fault structures inferred from balanced geologic cross sections. Both models for the northern and southern profiles indicate fault slip rates of about 44–46 mm/yr on the décollement and faults are nearly fully locked at shallow depths on the CYF, JMLF and CKF (Fig. 11c, d). These results

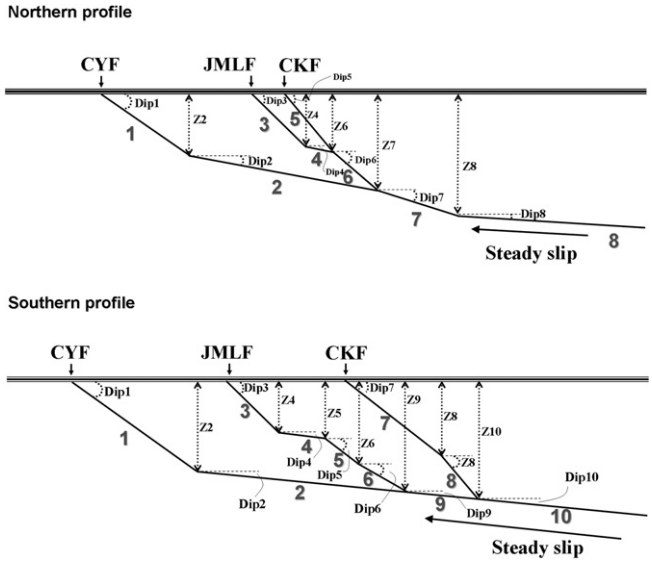

Fig. 9. The sketches of the fault geometries for two-dimensional fault models. (a) Northern profile, (b) southern profile. Model parameters of fault geometry and each sub-fault are shown. "Z" and "Dip" are fault depth and fault dip of each sub-fault. CYF, JMLF, and CKF denote the Chiayi Fault, Jiuchiunken–Muchiliao–Liuchia Fault system and Chukou Fault, respectively.

Table 4
The optimal model parameters for the two-dimensional fault model.

2D fault model		Optimal	95% Confi.	Average slip (mm/yr)
Northern profile $\chi^2 = 11$, *wrms* = 2.3 *mm/yr*				
Chiayi Fault	Dip1 (°)	20	17–22	S1 = 2.0
	Z1 (km)	1	0–2	
	Dip2 (°)	4	0–8	S2 = 3.7
	Z2 (km)	6	4–9	
Jiuchiunken Fault	Dip3 (°)	25	21–28	S3 = 0.01
	Z3 (km)	0	–	
	Dip4 (°)	11	9–15	S4 = 10.1
	Z4 (km)	3	1–4	
			44	
Chukou Fault	Dip5 (°)	28	22–31	S5 = 1.8
	Z5 (km)	0	–	
	Dip6 (°)	21	18–26	S6 = 12.3
	Z6 (km)	4	3–5	
Décollement	Dip7 (°)	13	9–15	S7 = 44.6
	Z7 (km)	8	6–10	
	Dip8 (°)	5	0–9	S8 = 46.2
	Z8 (km)	10	8–13	
Southern profile $\chi^2 = 12$, *wrms* = 2.3 *mm/yr*				
Chiayi Fault	Dip1 (°)	20	18–22	S1 = 3.6
	Z1 (km)	1	0–2	
	Dip2 (°)	12	8–15	S2 = 7.4
	Z2 (km)	6	4–7	
Liuchia Fault	dip3 (°)	30	25–32	S3 = 1.5
	Z3 (km)	0	–	
	Dip4 (°)	15	13–20	S4 = 7.3
	Z4 (km)	3	1–4	
	Dip5 (°)	25	19–27	S5 = 15.7
	Z5 (km)	4	3–7	
	Dip6 (°)	37	33–40	S6 = 17.5
	Z6 (km)	7	6–9	
Chukou Fault	Dip7 (°)	24	20–27	S7 = 2.0
	Z7 (km)	0	–	
	Dip8 (°)	36	30–38	S8 = 2.6
	Z8 (km)	5	3–7	
Décollement	Dip9 (°)	7	4–10	S9 = 25.1
	Z9 (km)	9	8–11	
	Dip10 (°)	7	4–10	S10 = 44.2
	Z10 (km)	10	11–13	

Note: Wrms is the model weighted root mean square value; χ^2 is the chi-square value, a mean value of normalized square residuals; dip, Z, and S indicate the fault dip, fault depth and slip rate on each subfault.

obtained from sufficient geological constraints are in agreement with results from the block model and buried dislocation model. Our study suggests a high potential for future large earthquakes in southwestern Taiwan. Given the interseismic slip rate of about 41–46 mm/yr on the fault and assume a recurrence interval of 150 years, future rupture may produce coseismic slip of about 6.1–6.9 m. Due to a high population density in southwestern Taiwan, the potential seismic hazard should not be overlooked.

7. Conclusions

The GPS velocity field between 1993 and 2007 in the Chiayi–Tainan area shows W-WNW directed motions with maximum rates of 33–44 mm/yr and decrease to 0–5 mm/yr near the coast. The remarkable subsidence of 31–59 mm/yr is observed in the Coastal Plain and is affected by the ground water withdrawal. Significant uplift rates of 5–20 mm/yr are also found at sites to the east of JMLF.

We use a block model, a buried dislocation model, and a two-dimensional fault model to invert for fault geometries and slip rates on major frontal thrust faults in the Chiayi–Tainan area. In the block model, the surface trace of JMLF is taken as a block boundary. The velocity of the eastern block is estimated to be 42 mm/yr in the direction of 280° with respect to the western block. We infer the fault locking depth of about 13 km, with a dip of 23° to the east. The maximum back-slip rate of 38 mm/yr near JMLF suggests that the fault is nearly fully locked at shallow depths.

The result from a buried dislocation model reveals a horizontal décollement at a depth of 8 km. The slip rate on the décollement is 41.6 mm/yr. If we connect the top edge of décollement to the surface trace of JMLF as a potential future rupture, it would suggest a 22° east-dipping fault.

The optimal 2D fault models constrained by balanced geologic cross sections require a gentle east-dipping décollement (5°–7°) at a depth of 10 km. The steady interseismic slip rate on the décollement is about 44–46 mm/yr, similar to that from the block model and buried dislocation model. Both the JMLF system and the Chukou Fault extend to the ground surface with dip of about 24°–30°, consistent with the geological observations. The Chiayi Fault is a blind thrust fault with the fault tip at 1 km depth and the dip of 20° to the east.

Results from various approaches show general agreement on fault geometries and slip rates. Our modeling results reveal that the JMLF system and other faults are nearly fully locked at shallow depths and suggest that the frontal thrust fault system in the Chiayi–Tainan area has a high potential for large earthquakes.

Acknowledgments

We are grateful to many colleagues at the Institute of Earth Sciences, Academia Sinica who have participated in collecting of survey-mode GPS data and maintaining the continuous GPS array. We thank Prof. Paul Segall of Stanford University for the permission to use some Matlab scripts on modeling crustal deformation. We also thank Dr. C.C.B. Yang and two anonymous reviewers for their valuable suggestion and comments. We are indebted to Central Weather Bureau (CWB), Ministry of the Interior (MOI), and Central Geological Survey (CGS) of Taiwan as well as International GNSS Service (IGS) community for providing the continuous GPS data in this study. This study was financially supported by the Academia Sinica and the National Science Council of Taiwan under grant NSC 97-2745-M-001-006. This is the contribution of the Institute of Earth Sciences, Academia Sinica, IESAS1657.

References

Angelier, J., 1986. Preface to the special issue on "Geodynamics of the Eurasian–Philippine Sea Plate boundary". Tectonophysics 125, IX–X.

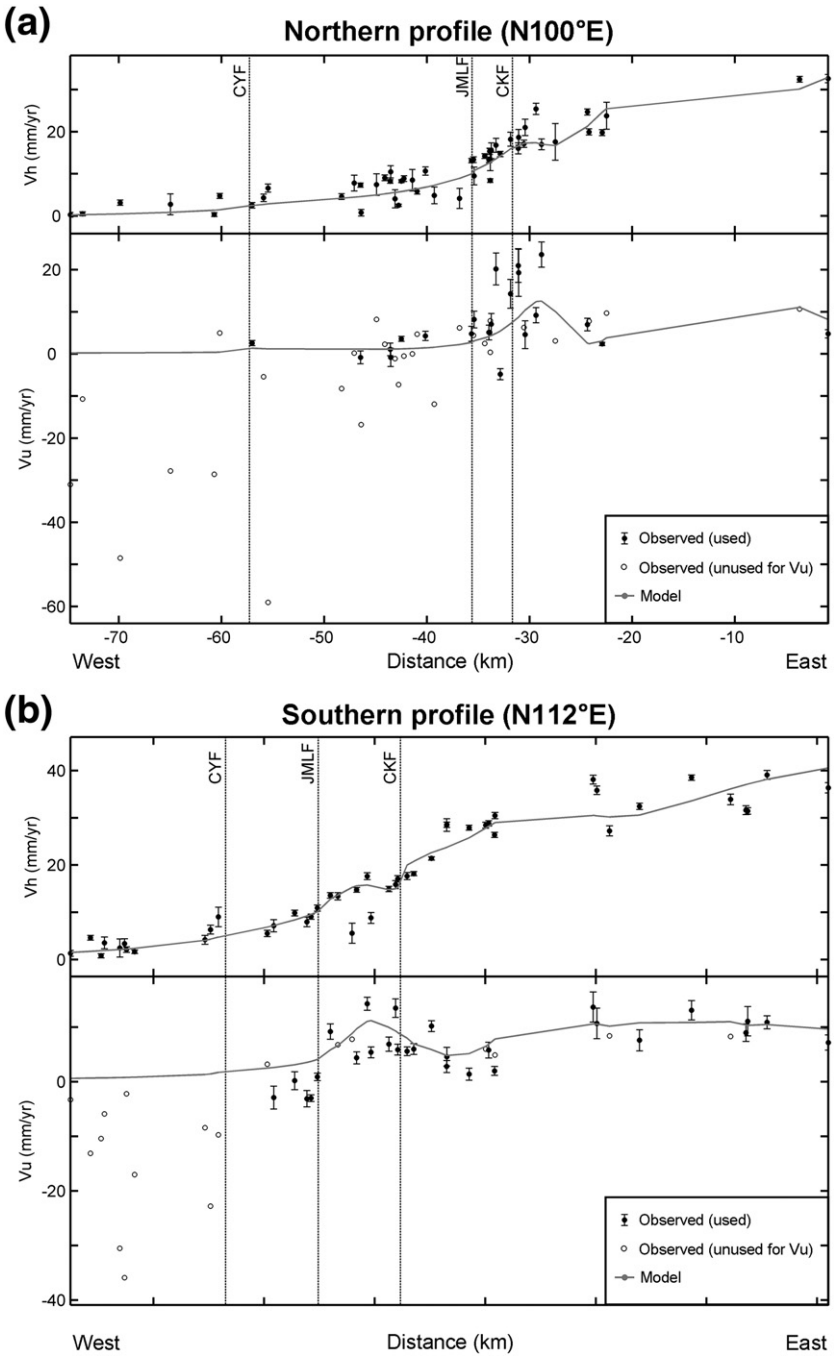

Fig. 10. The observed and predicted velocities in the northern and southern profiles from 2-dimensional fault models. (a) Northern profile (N100°E), (b) southern profile (N112°E). The location of these two velocity profiles are shown in Fig. 8. The dash lines indicate the surface positions of the Chiayi Fault (CYF), Jiuchiunken–Muchiliao–Liuchia Fault system (JMLF) and Chukou Fault (CKF). The solid circles with error bars denote the observed GPS velocities used in 2D fault model, while the hollow circles denote the unused vertical components. The thin curves represent the model-predicted velocity components.

Angelier, J., Barrier, E., Chu, H.T., 1986. Plate collision and paleostress trajectories in a fold–thrust belt: the Foothills of Taiwan. Tectonophysics 125, 161–178.
Bock, Y., 1994. Crustal deformation and earthquakes. Geotimes 39, 16–18.
Chen, R.F., 1999. Geomorphic index study of active structures in Chiayi-Tainan area, southwestern Taiwan (in Chinese with English abstract), M.S. thesis, National Cheng Kung Univ., Taiwan, 146 pp.
Chen, W.S., Yeh, M.G., Yang, C.C.B., Shih, R.C., Lin, C.W., 2006. Structural characteristics of the Meishan Fault (in Chinese). Bulletin of the Central Geological Survey Taiwan 19, 135–151.
Cheng, S.N., Yeh, Y.T., 2005. The distribution of earthquake fault and ground deformation in western Taiwan (in Chinese). Annual Meeting of the Geological Society of Taiwan, R.O.C.
Dixon, T.H., 1991. An introduction to the global position system and some geological applications. Review of Geophysics 29, 249–276.
Hager, B.H., King, R.W., Murray, M.H., 1991. Measurement of crustal deformation using the global position system. Annual Review of Earth and Planetary Sciences 19, 351–382.
Herring, T.A., King, R.W., McClusky, S.C., 2006a. GAMIT reference manual (analysis at MIT) release 10.3. Department of Earth, Atmospheric, and Planetary Sciences, Massachusetts Institute of Technology. (182 pp.).
Herring, T.A., King, R.W., McClusky, S.C., 2006b. GLOBK Reference Manual (Global Kalman Filter VLBI and GPS Analysis) Release 10.3. Department of Earth, Atmospheric, and Planetary Sciences, Massachusetts Institute of Technology. (91 pp.).
Hickman, J.B., Wiltschko, D.V., Hung, J.H., Fang, P., Bock, Y., 2002. Structure and evolution of the active fold-and-thrust belt of southwestern Taiwan from global positioning system analysis. In: Byrne, T.B., Liu, C.S. (Eds.), Geology and Geophysics of an Arc–Continent Collision, Taiwan: Boulder, Colorado: Geological Society of America Special Paper, 358, pp. 75–92.

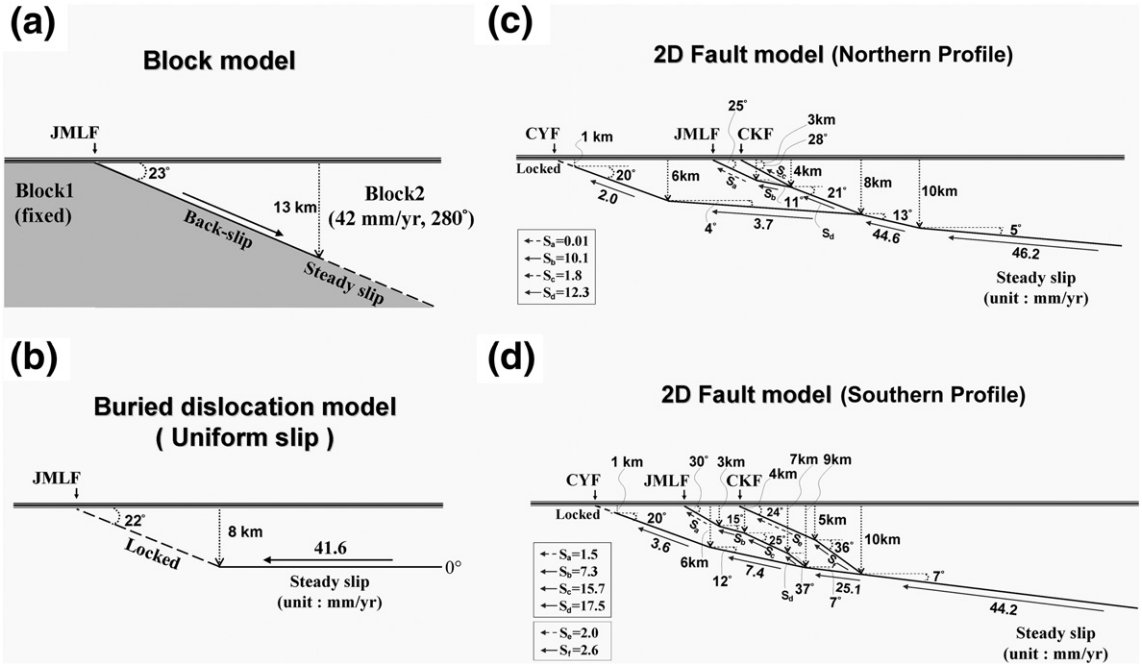

Fig. 11. A summary of the optimal fault parameters for four models in this study. (a) Block model, (b) buried dislocation model, (c) 2D fault model (northern profile), (d) 2D fault model (southern profile).

Ho, C.S., 1976. Foothills tectonics of Taiwan. Bulletin of the Central Geological Survey Taiwan 25, 9–28.

Ho, C.S., 2006. An introduction to the geology of Taiwan explanatory text of the geologic map of Taiwan. Bulletin of the Central Geological Survey, Taiwan.

Hsu, Y.J., Simons, M., Yu, S.B., Kuo, L.C., Chen, H.Y., 2003. A two-dimensional dislocation model for interseismic deformation of the Taiwan mountain belt. Earth and Planetary Science Letters 211, 287–294.

Hsu, S.K., Yeh, Y.C., Lo, C.L., Lin, A.T., Doo, W.-B., 2008. Linkage between crustal magnetization and earthquakes in Taiwan. Terrestrial Atmospheric and Oceanic Sciences 19, 445–450.

Hsu, Y.J., Yu, S.B., Simons, M., Kuo, L.C., Chen, H.Y., 2009. Interseismic crustal deformation in the Taiwan plate boundary zone revealed by GPS observations, seismicity, and earthquake focal mechanisms. Tectonophysics 479, 4–18.

Huang, G.T., 1996. Preliminary study on the tectonic geomorphology in the southwestern Foothills, Taiwan (in Chinese). M.S. thesis, National Central Univ., Taiwan, 114 pp.

Huang, S.T., 2003. Analysis of geological structure for fold and thrust belt in central and south Taiwan (in Chinese), Ph.D. dissertation, National Central University, Taipei, Taiwan, 129 pp.

Huang, C.S., Chang, H.C., Liu, H.C., 1995. The geological investigation of the Chukou Fault, southern Taiwan (in Chinese). Annual Report of Central Geological Survey.

Hudnut, K., 1995. Earthquake geodesy and hazard monitoring. Reviews of Geophysics 33, 249–255 (Suppl.).

Hugentobler, U., Schaer, S., Fridez, P., 2001. Bernese Software Version 4.2. Astronomical Institute, University of Berne. (515 pp.).

Hung, J.H., Wiltschko, D.V., Lin, H.C., Hickman, J.B., Fang, P., Bock, Y., 1999. Structure and motion of the southwestern Taiwan fold and thrust Belt. TAO 10, 543–586.

Johnson, H., 1995. Monument motion and measurements of crustal velocities. Geophysical Research Letters 22, 2905–2908.

Lacombe, O., Mouthereau, F., Anglier, J., Deffontaines, B., 2001. Structure, geodetic and seismological evidence for tectonic escape in SW Taiwan. Tectonophysics 333, 323–345.

Lallemend, S.E., Tsein, H.H., 1997. An introduction to active collision in Taiwan. Tectonophysics 274, 1–4.

Lee, T.Q., Angelier, J., 1995. Analysis of magnetic susceptibility anisotropy of the sedimentary and its tectonic implications. Paper Presented at International Conference and 3rd Sino–French Symposium on Active Collision in Taiwan, Geol. Soc. Of China, Taipei, March 22–23.

Lin, C.W., Chen, W.S., Liu, and Chen P.T., 2009. Active faults of eastern and southern Taiwan: Explanatory test for the strip maps of active faults, scale 1:25000 (in Chinese), Central Geological Survey Special publication no. 23, 174 pp.

Lin, A.T., Watts, A.B., Hesselbo, S.P., 2003. Cenozoic stratigraphy and subsidence history of the South China Sea margin in the Taiwan region. Basin Research 15 (4), 453–478.

Lin, C.W., Lu, S.T., Shih, T.S., Liu, Y.C., Lin, W.H., and Lin Y.C., 2007. Active faults of southwestern Taiwan: Explanatory test for the strip maps of active faults, scale 1:25000 (in Chinese), Central Geological Survey Special publication no. 17, 138 pp.

Liu, Y.C., Lin, Y.H., Lin, C.W., Lee, M.S., 2003. The Jiuchiunken fault. Annual Report of Central Geological Survey no.84, pp. 99–100.

Mao, A., Harrison, C.G.A., Dixon, T.H., 1999. Noise in GPS coordinate time series. Journal of Geophysical Research 104, 2797–2816.

Matsu'ura, M., Jackson, D.D., Cheng, 1986. A dislocation model for aseismic crustal deformation at Hollisater, California. Journal of Geophysical Research B12, P12661–12647 (November 10).

Matthews, M.V., Segall, P., 1993. Estimation of depth-dependent fault slip from measured surface deformation with application to the 1906 San Francisco earthquake. Journal of Geophysical Research 98, 12,153–112,163.

Mouthereau, F., Petit, C., 2003. Rheology and atrength of the Eurasian continental lithosphere in the foreland of the Taiwan collision belt: constraints from seismicity, flexure, and structural styles. Journal of Geophysical Research 108 (B11), 2512.

Nikolaidis, R., 2002. Observation of geodetic and seismic deformation with Global Positioning System, Ph.D. dissertation, Univ. of Calif., San Diego, 249pp.

Okada, Y., 1985. Surface deformation due to shear and tensile faults in a half-space. Bulletin of the Seismological Society of America 75, 1135–1154.

Omori, F., 1907a. Earthquake of the Chiayi area, Taiwan, 1906 (In Japanese) Introduction of Earthquake, pp. 103–147.

Omori, F., 1907b. Preliminary note on Formosa earthquake of March 17, 1906. Bull. Imp. Earthquake Investigation Committee, vol. 1, no. 2, pp. 53–59.

Savage, J.C., 1983. A dislocation model of strain accumulation and release at a subduction zone. Journal of Geophysical Research 88, 4984–4996.

Shyn, J.H., Sieh, K., 2005. Neotectonic architecture of Taiwan and its implications for future large earthquakes. Journal of Geophysical Research 110, B08402, http://dx.doi.org/10.1029/2004JB003251.

Shyn, J.H., Sieh, K., Chen, Y.G., 2005. Tandem suturing and disarticulation of the Taiwan orogen revealed by its neotectonic elements. Earth and Planetary Science Letters 233, 167–177.

Suppe, J., 1976. Decollement folding in southwestern Taiwan. Petroleum Geology of Taiwan 23, 25–35.

Suppe, J., 1980. Imbricate structure of western Foothills belt, south-central Taiwan. Petroleum Geology of Taiwan 17, 1–16.

Tsai, M.C., 2004. GPS time series analysis and modeling studies of the crustal deformation in southwestern Taiwan (in Chinese), Master dissertation, National Central University, Taipei, Taiwan, 103 pp.

Tsai, M.C., Yu, S.B., Chen, H.Y., 2007. A block model for the interseismic deformation in the Taiwan arc–continent collision zone. American Geophysical Union, Fall Meeting, Abstract, G12A-06.

Tsan, S.F., Keng, W.P., 1968. The Neogence rocks and major structure features of southwestern Taiwan. Petroleum of Geological Society of China 11, 45–49.

Williams, S., 2003. The effect of coloured noise on the uncertainties of rates estimated from geodetic time series. Journal of Geodesy 76, 483–494.

Yang, C.C.B., 2007. Seismogenic structure of the Chiayi-Tainan Area and the long-term slip rates of frontal thrusts in southwestern Taiwan, Ph.D. dissertation, National Taiwan University, Taipei, Taiwan, 116 pp.

Yang, K.M., Huang, S.T., Wu, J.C., Ting, H.H., Mei, W.W., 2006. Review and new insights on foreland tectonics in western Taiwan. International Geology Review 48, 910–941.

Yeh, M.G., Chen, W.S., Shyr, W.C., 1999. Seismic study of the Pliocene to Pleistocene series in the southwest plain, Taiwan (in Chinese). Petroleum Geology of Taiwan 33, 199–215.
Yu, S.B., Chen, H.Y., Kuo, L.C., 1997. Velocity field of GPS stations in the Taiwan area. Tectonophysics 274, 41–59.
Yu, S.B., Kuo, L.C., Punongbayan, R.S., Ramos, E.G., 1999. GPS observation of crustal motion in the Taiwan–Luzon region. Geophysical Research Letters 26, 923–926.
Zhang, J., Bock, Y., Johnson, H., Fang, P., Williams, S., Genrich, J., Wdowinski, S., Behr, J., 1997. Southern California permanent GPS geodetic array: error analysis of daily position estimates and site velocities. Journal of Geophysical Research 102, 18,035–18,055.